Nanoscale

ELECTRONIC SUPPORTING INFORMATION

Upconversion thermometry: a new tool to measure the thermal resistance of nanoparticles

O. A. Savchuk,[a] J. J. Carvajal,[a]* C. D. S. Brites,[b] L. D. Carlos,[b]* M. Aguilo,[a] F. Diaz

[a]Fisica i Cristal.lografia de Materials i Nanomaterials (FiCMA-FiCNA) – EMaS, Universitat Rovira i Virgili (URV), Campus Sescelades, Marcel.li Domingo 1, E-43007 Tarragona, Spain.
[b]Department of Physics, CICECO – Aveiro Institute of Materials, University of Aveiro, Campus Universitário de Santiago, 3810-193 Aveiro, Portugal.

*Corresponding Authors: lcarlos@ua.pt; joanjosep.carvajal@urv.cat

1. XRD

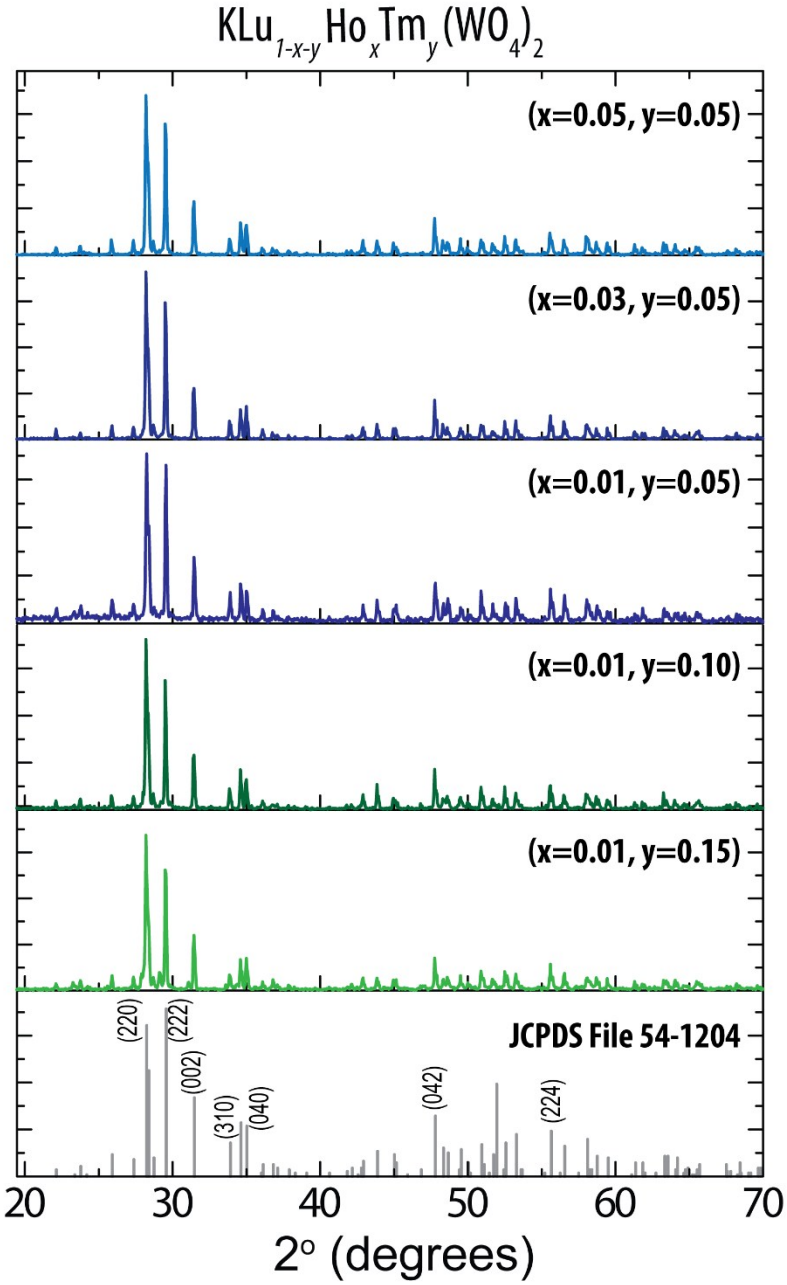

Figure S1. XRD patterns of the $KLu_{1-x-y}Ho_xTm_y(WO_4)_2$ nanoparticles) (x=0.01, 0.03, 0.05 and y=0.05, 0.10, 0.15). The patterns were acquired in a Bruker-AXS D8-Discover diffractometer using Cu K_α radiation. The reference XRD pattern, corresponding to $KLu(WO_4)_2$ (JCPDS file 54-1204), is included for comparison.

2. Elemental analysis

Table S1 presents the elemental analysis for Ho, Tm and Lu, that were performed by inductively coupled plasma optical emission spectroscopy (ICP-OES) on a Jobin Yvon Activa-M instrument with a glass concentric nebulizer. The samples were digested under microwaves with 0.5 mL of hydrochloric acid (HCl) and 1 mL of nitric acid (HNO_3). After being digested under microwaves, the samples were recovered in 50 mL of ultrapure water. The method is accurate within 10 %.

Table S1. ICP-OES analysis of the dopant concentration of $KLu(WO_4)_2$:Ho^{3+},Tm^{3+}:nanoparticles synthesized by the Pechini method.

Material $KLu_{1-x-y}Ho_xTm_y(WO_4)_2$	Ho (w/w %) *x* (%)	Tm (w/w %) *y* (%)	Lu (w/w %) *1-x-y* (%)
***x=0.01, y*=0.05**	0.93	4.9	94.17
***x=0.03, y*=0.05**	2.2	3.57	94.22
***x=0.05, y*=0.05**	5.08	5.16	89.75
***x=0.01, y*=0.15**	0.98	11.57	87.44

3. Upconversion mechanism

The following tentative mechanism explains the Tm^{3+} and Ho^{3+} upconverting emission, Figure 2c. For Tm^{3+}, the 808 nm radiation excites electrons to the $^3H_4$ level from where they non-radiatively relax to the $^3F_4$ level. From here, the absorption of a second photon at 808 nm promotes the electrons to the $^1G_4$ level, from which they relax radiatively to the $^3H_6$ ground state, generating the emission at 475 nm. Another possibility is the non-radiative decay from the $^1G_4$ level to the $^3F_{2,3}$ levels, from which can occur a radiative transition to the ground state, generating the emission at 695 nm.

The energy levels of Ho^{3+} can be populated through: (i) energy transfer between the Tm^{3+} $^3H_4$ level to the Ho^{3+} $^5I_5$ level and (ii) energy transfer from the $^3F_4$ manifold of Tm^{3+} to the $^5I_7$ manifold of Ho^{3+}, from which also an energy back transfer process to Tm^{3+} can occur.

Besides the direct energy transfer from Tm^{3+}, the $^5I_7$ level of Ho^{3+} can also be populated by the non-radiative relaxation from the $^5I_5$ energy level. Also, from the $^5I_7$ level of Ho^{3+}, the transfer of energy of a photon at 808 nm from Tm^{3+} promotes the electrons of Ho^{3+} to the higher energy levels $^3K_8$ and $^5F_3$. From these levels non-radiative decays populate the $^5S_2$ and $^5F_4$ levels resulting in a radiative transition towards the $^5I_7$ level (emission at 755 nm), and/or towards the $^5I_8$ ground state (emission at 545 nm). Finally, a radiative transition from the $^5F_5$ level, which is populated from the non-radiative relaxation of the $^3K_8$ and $^5F_3$ energy levels, to the $^5I_8$ ground state, generated the emission at 650–660 nm.

4. Thermometric characterization

Table S2. Calibration curves fitting parameters for the $KLu_{1-x-y}Ho_xTm_y(WO_4)_2$ nanoparticles containing different dopant concentrations, accordingly to Eq.1 of the manuscript.

Sample	Δ_0	B	α (K^{-1})	r^2
$KLu_{0.94}Ho_{0.01}Tm_{0.05}(WO_4)_2$	−1.63	0.32	0.007	*0.999*
$KLu_{0.92}Ho_{0.03}Tm_{0.05}(WO_4)_2$	1.19	−1.47	−0.07	*0.998*
$KLu_{0.90}Ho_{0.05}Tm_{0.05}(WO_4)_2$	1.30	−1.15	−0.06	*0.998*
$KLu_{0.84}Ho_{0.01}Tm_{0.15}(WO_4)_2$	1.36	−1.13	−0.081	*0.998*

5. Photothermal heating efficiency

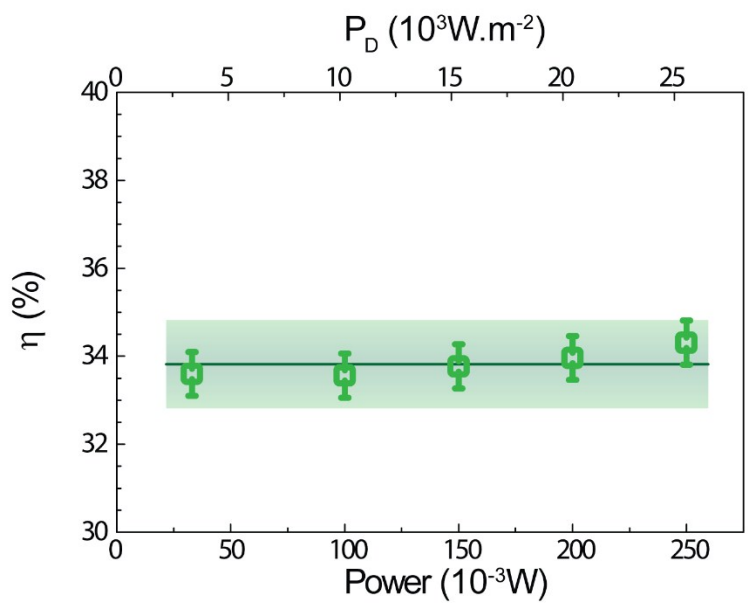

Figure S2. Photothermal conversion efficiency of the $KLu_{0.84}Ho_{0.01}Tm_{0.15}(WO_4)_2$ nanoparticles for distinct excitation power density values. Solid line and the shadowed area represent, respectively, the mean value and the standard deviation.

Table S3. The photothermal conversion efficiency of $KLu_{0.84}Ho_{0.01}Tm_{0.15}(WO_4)_2$ nanoparticles compared with other systems. The heating wavelength (λ) and the pumping power (P) of the laser together with the photothermal efficiency (η) reported are listed for comparison.

Material	λ (nm)	P (W)	η(%)	Method†	Ref.
$NdVO_4$ nanoparticles	808	0.403	72	**TR**	[1]
$NaNdF_4$@$NaYF_4$@1%Nd^{3+}:$NaYF_4$ multishell nanostructures	808	*	73	**TR**	[2]
Graphene in DMF	808	0.2	67	**IS**	[3]
Au nanorods	815	0.15	61	**TR**	[4]
Au/AuS nanoshells	815	0.16	59	**TR**	[4]
Graphene oxide in water	808	0.2	58	**IS**	[3]
Au nanorods	808	2	50	**TR**	[5]
Dopamine-melanin	808	2	40	**TR**	[6]
Biodegradable Au nanovesicles	808	1	37	**TR**	[7]
$KLu_{0.84}Ho_{0.01}Tm_{0.15}(WO_4)_2$	808	0.2	34	**IS**	This work
	808	0.2	41	**TR**	This work
Au/SiO_2 nanoshells	815	0.16	34	**TR**	[4]
FePt nanoparticles	800	-	30	**PR**	[8]
Cu_9S_5	980	0.51	25.7	**TR**	[9]
Au nanoshell	808	2	25	**TR**	[10]
$Cu_{2-x}Se$ nanoparticles	800	2	22	**TR**	[11]
Au nanorods	808	1	22	**TR**	[7]
Au nanoshells	808	1	18	**TR**	[7]

***IS**: integrating sphere; **TR**: thermal relaxation, **PR**: $P_{\text{converted to heat}}/P_{\text{excitation}}$*

* No power value was reported. The value presented is the laser power density, 2.0 W·cm^{-2}.

Calculating the photothermal heat efficiency using Eq. 4 of the manuscript:

The thermal capacitance of the system, C=2.936 J·K^{-1}, is calculated using the data presented in Table S4.

Table S4. Thermal capacitance of the system and mass (*m*) and specific heat capacity (*c*) of all their *i* components.

Component	*c* (J·kg^{-1}·K^{-1})	*m* (kg)	*c*×*m* (J·K^{-1})	*C* (J·K^{-1})
$KLu_{0.84}Ho_{0.01}Tm_{0.15}(WO_4)_2$	324	7.2×10^{-12}	2.35×10^{-9}	
Water	4815.5	3.0×10^{-4}	1.256	
Glass cuvette	840	2.0×10^{-3}	1.680	
				2.936

The absorbance of the suspension (A_λ) is calculated using the values of the incident and transmitted power for the system at λ=808 nm. As the incident power is I=0.200 W and the transmitted power is 0.022 W, then the absorbed power is I_{abs}=0.178 W and the corresponding A_λ is given by:

$$A_\lambda = -\log_{10}\left(1-\frac{I}{I_{abs}}\right) \quad \text{(S1)}$$

resulting A_λ=0.959. The error in the photothermal heating efficiency is:

$$\Delta\eta = \sqrt{\left(\frac{\frac{C}{\tau}\Delta(T_m-T_a)}{I\left(1-10^{-A_\lambda}\right)}\right)^2 + \left(\frac{\frac{C\,(T_m-T_a)}{\tau^2}\Delta\tau}{I\left(1-10^{-A_\lambda}\right)}\right)^2} \times 100\ \% \quad \text{(S2)}$$

where $\Delta(T_m\text{-}T_a)$=0.05 K results from the fluctuations of the measured temperature values in the steady regime, and $\Delta\tau$=0.7 s is the error resulting from the OriginLab® fitting software. The resulting error is 0.06 % and so the error in the method (3 %) was considered.

6. Modeling the temperature evolution of irradiated nanoparticles

To model the temperature increase measured by the nanoparticles upon 808 nm excitation, we first compute the Biot Number for the nanoparticles:

$$Bi = \frac{hL_c}{\kappa} \quad \text{(S4)}$$

where h is the convective heat transfer coefficient (h=10–100 W·m^{-2}·K^{-1}, typically for quiescent air[12]), κ is the thermal conductivity of the nanoparticles and L_c is its characteristic length. Using the κ value of the $KLu(WO_4)_2$ crystal co-doped with Tm^{3+} and Yb^{3+}, 2.2 W·m^{-1}·K^{-1} [13], and L_c of the order of 1–100×10^{-7} m, results that $5\times10^{-7} \leq Bi < 5\times10^{-4}$. As Bi<0.1, the nanoparticle can be considered as a lumped system to model the energy transfer to the surrounding media (Figure S3), implying that the thermal gradients within the nanoparticle is negligible when compared with the temperature change in its neigboroud.[12]

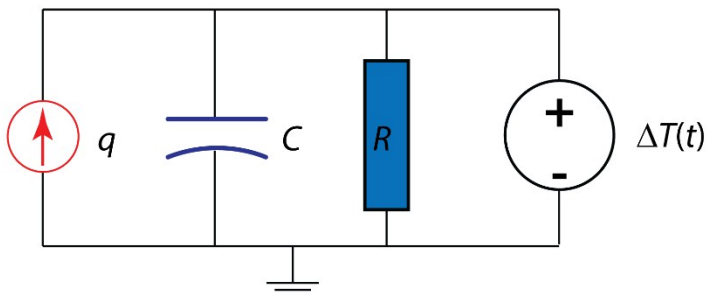

Figure S3. Equivalent thermal circuit used to model the temperature increase on the nanoparticles exposed to laser irradiation. The heat absorbed by the nanoparticles (q) is dissipated by air convection (through the thermal resistance R) and determined by the thermal capacitance (C) of the nanoparticles. The real-time temperature increase measured by the nanoparticles (ΔT) is described by Eq. 9.

Notice that the maximum temporal change of the temperature profile, be used to compute the temporal resolution, can be calculated as:

$$\left|\frac{dT}{dt}\right|_{max} = \left|\frac{d\Delta T}{dt}\right|_{max} = \left|\frac{\Delta T_m\left(1-\exp\left(-\frac{t}{\tau}\right)\right)}{dt}\right|_{max} = \frac{\Delta T_m}{\tau} \quad \text{(S5)}$$

7. References

1. B. del Rosal, A. Perez-Delgado, E. Carrasco, D. J. Jovanovic, M. D. Dramicanin, G. Drazic, A. J. de la Fuente, F. Sanz-Rodriguez and D. Jaque, *Adv. Opt. Mater.*, 2016, **4**, 782-789.
2. L. Marciniak, A. Pilch, S. Arabasz, D. Jin and A. Bednarkiewicz, *Nanoscale*, 2017, **9**, 8288–8297.
3. O. A. Savchuk, J. Carvajal, J. Massons, M. Aguiló and F. Díaz, *Carbon*, 2016, **103**, 134-141.
4. J. R. Cole, N. A. Mirin, M. W. Knight, G. P. Goodrich and N. J. Halas, *J. Phys. Chem. C*, 2009, **113**, 12090-12094.
5. W. Xu, X. Gao, L. Zheng, Z. Zhang and W. Cao, *Sensor Actuat. B Chem.*, 2012, **173**, 250-253.
6. Y. Liu, K. Ai, J. Liu, M. Deng, Y. He and L. Lu, *Adv. Mater.*, 2013, **25**, 1353-1359.
7. P. Huang, J. Lin, W. Li, P. Rong, Z. Wang, S. Wang, X. Wang, X. Sun, M. Aronova and G. Niu, *Angew. Chem.-Int. Edit.*, 2013, **52**, 13958-13964.
8. Z. Chen, W. Sun, H. J. Butt and S. Wu, *Chem. Eur. J.*, 2015, **21**, 9165-9170.
9. Q. Tian, F. Jiang, R. Zou, Q. Liu, Z. Chen, M. Zhu, S. Yang, J. Wang, J. Wang and J. Hu, *ACS Nano*, 2011, **5**, 9761-9771.
10. V. P. Pattani and J. W. Tunnell, *Lasers Surg. Med.*, 2012, **44**, 675-684.
11. C. M. Hessel, V. P. Pattani, M. Rasch, M. G. Panthani, B. Koo, J. W. Tunnell and B. A. Korgel, *Nano Lett.*, 2011, **11**, 2560-2566.
12. F. P. Incropera, D. P. DeWitt, T. L. Bergman and A. S. Lavine, *Introduction to Heat Transfer*, Wiley, New York, 5 edn., 2006.
13. H. Y. Zhao, J. Y. Wang, J. Li, J. X. Zhang, H. J. Zhang and M. H. Jiang, *J. Cryst. Growth*, 2006, **293**, 223-227.